Infection and Drug Resistance

Dovepress
Taylor & Francis Group

Open Access Full Text Article

ORIGINAL RESEARCH

Integrated Proteomics and Metabolomics Reveal Multifaceted Mechanisms of Colistin Resistance in *Acinetobacter baumannii*

Ling Hao[1,2], Xiao Yang[3], Nadeem Ullah[4], Yujun Li[1], Shuquan Wei[1], Qizhi Wang[1], Zhuxiang Zhao[1], Zhike Liang[1]

[1]Department of Pulmonary and Critical Care Medicine, Guangzhou First People's Hospital, South China University of Technology, Guangzhou, People's Republic of China; [2]Institute of Clinical Medicine, Guangzhou First People's Hospital, South China University of Technology, Guangzhou, People's Republic of China; [3]Department of Laboratory Medicine, Guangzhou First People's Hospital, South China University of Technology, Guangzhou, People's Republic of China; [4]Department of Clinical Microbiology, Umeå University, Umeå, Sweden

Correspondence: Zhuxiang Zhao; Zhike Liang, Email zhaozhuxiang@126.com; eylzk@scut.edu.cn

Background: The emergence of colistin-resistant *Acinetobacter baumannii*, particularly extensively drug-resistant carbapenem-resistant *A. baumannii* (XDR-CRAB), poses a critical global health threat; however, the molecular mechanisms underlying this resistance remain poorly characterized.

Methods: This study utilized integrated tandem mass tag (TMT)-based proteomics and untargeted metabolomics to compare a representative drug-sensitive (DS) strain, a colistin-sensitive multidrug-resistant (MDR-CRAB) strain, and a colistin-resistant extensively drug-resistant (XDR-CRAB) isolate from a Guangzhou hospital, China, with a primary focus on the molecular features associated with resistance in the XDR isolate.

Results: Proteomic analysis identified 260 differentially expressed proteins (DEPs) across these strains, with 98 strongly linked to the colistin-resistant phenotype. These DEPs were enriched in functions related to polysaccharide and sulfate transport, aromatic compound degradation, and cationic antimicrobial peptide (CAMP) resistance. Upregulation of the lipid A modification system, driven by increased expression of PmrA (4.2-fold), PmrB (2.9-fold), and PmrC (5.5-fold) in the XDR strain compared to the MDR strain, is consistent with this CAMP resistance. Metabolomic analysis identified 747 metabolites, with lipids and lipid-like molecules being the most altered class. The XDR strain exhibited reduced relative abundance of several glycerophospholipids and fatty acids/conjugates, when compared to the MDR strain, indicating cell membrane remodeling. Pathway enrichment analysis further implicated purine, glycerophospholipid, starch/sucrose, and glutathione metabolism in colistin resistance.

Conclusion: Colistin resistance in *A. baumannii* appears to involve a multifaceted strategy integrating lipid A modification, cell membrane remodeling, and metabolic reprogramming. This study provides a high-resolution molecular blueprint of colistin resistant *A. baumannii* and generates testable hypotheses to inform future diagnostic and therapeutic strategies against resistant infections.

Keywords: *Acinetobacter baumannii*, multidrug-resistant, extensively drug-resistant, colistin, carbapenem, quantitative proteomics, untargeted metabolomics, lipid A modification

Introduction

Acinetobacter baumannii (*A. baumannii*), a member of the ESKAPE pathogens (*Enterococcus faecium, Staphylococcus aureus, Klebsiella pneumoniae, A. baumannii, Pseudomonas aeruginosa*, and *Enterobacter* spp.), has emerged as a critical opportunistic pathogen causing both nosocomial and community-acquired infections.[1] Most *A. baumannii* isolates exhibit multidrug resistance (MDR) and predominantly affect vulnerable patient populations, resulting in alarming mortality rates (40~84.3%).[2,3] National surveillance data in China ranks *A. baumannii* as the second most prevalent pathogen isolated from respiratory tract (13.0%) and cerebrospinal fluid (12.3%) specimens.[4] A concerning trend reveals carbapenem resistance steadily climbed between 2005 and 2023: meropenem resistance increased from 39.0% to 73.7%, and imipenem resistance

https://doi.org/10.2147/IDR.S573066
Received: 31 October 2025
Accepted: 22 January 2026
Published: 3 February 2026

rose from 31.0% to 73.4% over the same two-decade span.[4] Although 2024 data showed modest declines (meropenem 64.7%; imipenem 64.5%), *A. baumannii* maintains carbapenem resistance rates 28~32 times higher than *Escherichia coli*, 3~4 times higher than *Pseudomonas aeruginosa*, and nearly triple those of *Klebsiella pneumoniae* (2024 CHINET surveillance data). Most critically, the rapid acquisition of extensively drug-resistant (XDR) and pan-drug-resistant (PDR) phenotypes in *A. baumannii* represents a global health emergency requiring urgent intervention.[1]

Carbapenem-resistant *A. baumannii* (CRAB) in Guangdong Province, southern China, is more prevalent than in neighboring provinces, with a 2022 surveillance detection rate of 78.5% versus 60.4% in Hunan and 60.3% in Fujian.[4] Colistin serves as the last-resort treatment for CRAB infections.[5] Although current colistin resistance rates remain low, expanding clinical use correlates with progressive increases in resistance to this critical agent. Critically, colistin-resistant strains often co-harbor other resistance genes, leading to XDR and PDR phenotypes that severely limit treatment options.[6] These complex resistance profiles stem from *A. baumannii*'s principal resistance mechanisms, including enzymatic antibiotic inactivation, outer membrane permeability barriers, active efflux pump systems, and target site mutations.[7] Colistin resistance specifically arises through two principal mechanisms targeting lipopolysaccharides (LPS).[8–10] As a cationic peptide, colistin normally binds to the negatively charged lipid A component of LPS via electrostatic interactions.[11] Resistance develops either through complete LPS loss caused by mutations in *lpxACD* genes (essential for lipid A biosynthesis), or through structural modification of LPS involving phosphoethanolamine (PEtN) addition to lipid A, a process mediated by *pmrCAB*-encoded enzymes.[8–10] These alterations reduce the outer membrane's negative charge, thereby diminishing colistin's electrostatic binding capacity. Beyond chromosomal determinants, plasmid-borne PEtN transferases (*mcr-1* to *mcr-8*) significantly amplify colistin resistance by facilitating rapid horizontal dissemination of resistance phenotypes.[12] Moreover, emerging evidence highlights the broader role of bacterial metabolism in resistance development. For instance, amino acid metabolism may confer environmental stress tolerance through intracellular pH homeostasis, energy production, and motility reduction.[13] Similarly, carbohydrate metabolic pathways contribute to biofilm formation and maintenance, consequently influencing drug resistance evolution.[14] Nevertheless, the specific metabolic adaptations underlying colistin resistance remain poorly characterized.

Driven by concerns arising from the post-COVID-19 emergence of colistin-resistant *A. baumannii* and its potential link to increased mortality within our respiratory department at a tertiary hospital in Guangzhou, Guangdong,[15] we conducted an in-depth, comparative multi-omics analysis. This study examined drug-sensitive (DS), colistin-sensitive MDR-CRAB, and colistin-resistant XDR-CRAB clinical *A. baumannii* strains isolated from our hospital between November 2022 and January 2023. Using tandem mass tag (TMT)-based quantitative proteomics coupled with LC-MS/MS metabolomics, this study aimed to provide a high-resolution molecular blueprint and elucidate the key biological processes underlying colistin resistance.

Materials and Methods

Bacterial Strains and Culture

Three *A. baumannii* clinical strains, designated as DS, MDR and XDR, were obtained from the clinical microbiology laboratory of Guangzhou First People's Hospital (Guangzhou, China). These isolates were collected from different inpatients between November 2022 and January 2023 as part of routine hospital procedures without involvement of any external institution. All bacterial isolates were anonymized and processed without any patient identifiers. Species identification was confirmed using biochemical tests combined with the IVD MALDI Biotype system (Bruker Daltonics, GmbH and Co., Bremen, Germany). All isolates were cultured in LB broth to mid-log phase, washed twice with cold PBS. Samples were flash-frozen in liquid nitrogen and stored at −80°C until further processing for proteomics (3 replicates per strain) and metabolomics (6 replicates per strain) analysis.

Antimicrobial Susceptibility Testing

Antimicrobial susceptibility profiles were determined using the Vitek-2 Compact automated system (bioMérieux, Marcy-l'Étoile, France). Colistin susceptibility for all strains was further verified by broth microdilution method according to Clinical and Laboratory Standards Institute (CLSI) guidelines (M100, 33rd Edition) as described previously.[16] Quality control strains *Escherichia coli* ATCC 25922 and *Pseudomonas aeruginosa* ATCC 27853 were included in all assays.

Protein Extraction and Digestion

The cell pellets were pulverized and resuspended in ice-cold lysis buffer (4% SDS, 10 mM dithiothreitol [DTT], 100 mM triethylammonium bicarbonate [TEAB], 100 mM NaCl), followed by sonication for 5 min on ice. Supernatants were collected by centrifugation (12,000 × g, 4°C, 15 min) and alkylated with 0.5 M iodoacetamide (IAM) for 1 h in the dark. Proteins were precipitated using four volumes of pre-chilled acetone (−20°C, 2 h), washed with 1 mL of cold acetone, and resolubilized in dissolution buffer (8 M urea, 100 mM TEAB, pH 8.5). Finally, protein samples were digested with trypsin at a ratio of 1:80 (4 h, 37°C) followed by 1:40 (overnight, 4°C).

TMT Labeling and Peptide Fractionation

The resulting peptide digests were desalted using a C18 solid-phase extraction column (Phenomenex, Torrance, CA, United States) and lyophilized. Dried peptides were reconstituted in 0.1 M TEAB (Sigma), labeled with TMT isotopes (Table S1), combined equally, desalted, and vacuum-dried. Fractionation was performed on a Rigol L-3000 HPLC system with a C18 column (Waters BEH C18, 5 μm particle size, 4.6 mm ID, 250 mm length) at 1 mL/min, using a 60 min gradient from 3–100% Buffer B (98% acetonitrile) and collecting ten fractions. Fractions were vacuum-centrifuged and reconstituted in 0.1% formic acid.

UHPLC-MS/MS Peptide Analysis

UHPLC-MS/MS analysis was conducted on an EASY-nLC 1200 system coupled to a Q Exactive^{TM} HF-X mass spectrometer (Thermo Fisher, Dreieich, Germany) at Novogene Co.,Ltd. (Beijing, China). Peptides were separated on a homemade analytical column (1.9 μm particle size, 75 μm ID, 250 mm length) at 600 nL/min using a gradient of 6–100% Solvent B (80% acetonitrile, 0.1% formic acid) over 60 min. MS acquisition parameters included: full MS scan range 350–1500 m/z (60,000 resolution); top 40 precursors selected for higher-energy collisional dissociation (HCD) fragmentation (MS/MS resolution 30,000 at 200 m/z); 54 ms maximum injection time; 20s dynamic exclusion.

TMT Protein Identification and Quantification

Raw data files were processed using Proteome Discoverer 2.5 (Thermo Fisher) against the Uniprot *A. baumannii* database (Taxon ID:470, updated on 27 September 2023). Search parameters included: 10 ppm precursor/0.02 Da product mass tolerance; trypsin digestion with ≤2 missed cleavages; fixed carbamidomethylation (C); variable methionine oxidation and TMT modifications. Proteins required ≥1 unique peptide with false discovery rate (FDR) <1%. The thresholds of fold change (FC) >2 or <0.5 and $p < 0.05$ were used to identify differentially expressed proteins (DEPs).

Metabolite Extraction

Metabolites were extracted using ice-cold 80% methanol with vortexing (30 s) and ultrasonication (6 min, ice-water bath). After centrifugation (12,000 rpm, 15 min, 4°C), supernatants were lyophilized and reconstituted in 10% methanol for analysis. Quality control (QC) samples were prepared by pooling equal volumes of supernatant from all extracts.

UHPLC-MS/MS Metabolite Analysis

Metabolites were analyzed on a Vanquish UHPLC system coupled to an Orbitrap Q Exactive^{TM} HF-X mass spectrometer (Thermo Fisher) at Novogene Co.,Ltd. (Beijing, China). Eluent A contained 0.1% formic acid (positive mode) or 5 mM ammonium acetate (pH 9.0, negative mode), while Eluent B was methanol for both modes. Separation was performed on a Hypersil Gold C18 column (2.1 × 100 mm, 1.9 μm) at 0.2 mL/min with this gradient: 2% B (1.5 min), 2–85% B (3 min), 85–100% B (10 min), 100–2% B (10.1 min), 2% B (23 min). MS settings included alternating positive/negative ionization modes, 3.5 kV spray voltage, 320°C capillary temperature, sheath/aux gas flows (35/10 arbitrary units), S-lens RF level 60, and 350°C auxiliary gas heater.

Metabolite Identification

Raw metabolomics data were processed using Compound Discoverer 3.3 (Thermo Fisher) with total spectral intensity normalization for peak alignment and quantification. Metabolites were annotated by predicting molecular formulas and hybrid database matching against online mzCloud database (https://www.mzcloud.org/, accessed October 26, 2023) and in-house libraries (mzVault/MassList). QC-filtered metabolites (coefficient of variation (CV) ≤ 30%) were further annotated through the Kyoto Encyclopedia of Genes and Genomes (KEGG) (http://www.genome.jp/kegg/) and ClassyFire (http://classyfire.wishartlab.com/) databases. Principal component analysis (PCA) was performed using MetaX to reveal inter-group metabolic variations. The significant differentially expressed metabolites (DEMs) between the comparison groups were identified by variable importance in the projection (VIP) > 1, FC > 2 or < 0.5, and $p < 0.05$.

Statistical and Bioinformatic Analysis

Statistical analyses were performed using using IBM SPSS Statistics (version 20.0; SPSS Inc., Chicago, IL, USA). Two-tailed Student's *t*-test was used for two-group comparison. Functional and pathway annotation of identified proteins was performed using the Gene Ontology (GO) and KEGG databases. Volcano plots were generated using the R package ggplot2. Fuzzy c-means clustering was performed using the R package Mfuzz. Enrichment analyses of DEPs for GO terms and KEGG pathways were performed separately using the R package clusterProfiler. Terms with a $p < 0.05$ were considered significantly enriched. Pathway enrichment analysis of the DEMs was performed using MetaboAnalyst 6.0 web platform (https://www.metaboanalyst.ca/home.xhtml).

Results

Susceptibility Profiles of the DS, MDR, and XDR Strains

The antibiotic susceptibility profiles of the three *A. baumannii* clinical isolates were summarized in Table 1. Both MDR and XDR strains exhibited resistance to carbapenems (imipenem MIC ≥ 16 μg/mL; meropenem MIC ≥ 16 μg/mL), while all strains remained sensitive to tigecycline (MIC ≤ 2 μg/mL). Notably, the XDR strain demonstrated high-level colistin resistance (MIC = 64 μg/mL), exceeding the CLSI susceptibility breakpoint (≤2 μg/mL).

Table 1 MICs of Commonly Used Clinical Antibiotics Against DS, MDR, and XDR Clinical Isolates

Antibiotics	MICs of Strains (μg/mL)		
	DS	MDR	XDR
Cefepime	2	≥ 32	16
Cefoperazone/Sulbactam	≤ 8	≥ 64	≥ 64
Ceftazidime	2	≥ 64	≥ 64
Ciprofloxacin	≤ 0.25	≥ 4	≥ 4
Colistin	0.5	1	64
Doxycycline	≤ 0.5	≥ 16	≥ 16
Imipenem	≤ 0.25	≥ 16	≥ 16
Levofloxacin	≤ 0.12	≥ 8	≥ 8
Meropenem	≤ 0.25	≥ 16	≥ 16
Minocycline	≤ 1	8	≥ 16
Piperacillin/Tazobactam	≤ 4	≥ 128	≥ 128
Ticarcillin/Clavulanic acid	≤ 8	≥ 128	≥ 128
Tigecycline	≤ 0.5	2	2
Tobramycin	≤ 1	≥ 16	≥ 16
Trimethoprim/Sulfa	≤ 20	≥ 320	≥ 320

Identification of DEPs Across Resistance Phenotypes

A total of 3,148 proteins were identified across the three strains using TMT-based quantitative proteomics. Data quality was validated by peptide coverage, protein sequence coverage, molecular weight distribution, and peptide length distribution (Figure S1). Comparative analysis identified 260 DEPs (8.3% of total) meeting the criteria: $p < 0.05$, FC > 2 or < 0.5. Specifically, the MDR strain showed 70 up-regulated and 26 down-regulated proteins compared to the DS strain (Figure 1A), while the XDR strain had 88 up-regulated and 17 down-regulated proteins (Figure 1B). Between the XDR and MDR strains, 201 DEPs were identified, with 117 higher and 84 lower in the XDR strain (Figure 1C). DEPs for each comparison were detailed in Tables S2–S4.

Colistin Resistance-Associated Protein Signatures in the XDR Strain

Heatmap analysis demonstrated distinct proteomic clustering among the three strains (Figure 2A). To explore potential colistin resistance mechanisms and screen for novel biomarkers in *A. baumannii*, fuzzy c-means clustering analysis was performed based on relative protein abundance profiles. The 260 DEPs were assigned to six clusters (Figure 2B, Table S5), with primary focus on Cluster 1 (73 proteins) and Cluster 2 (25 proteins) due to their significantly increased/decreased levels in the XDR strain compared to the MDR and DS strains. GO functional enrichment analysis of these key clusters identified significant involvement in polysaccharide transport, catechol-containing compound metabolic process, sulfate transport, and response to stimulus for biological processes (shown in orange in Figure 3A). The molecular functions focused on multiple enzymes/transmembrane transporters (shown in blue in Figure 3A). KEGG analysis linked DEPs to degradation and metabolism of aromatic compounds, nucleotides, amino acids, and phosphonates/phosphinates, as well as cationic antimicrobial peptide (CAMP) resistance (Figure 3B). Notably, the lipid A modification system PmrA (4.2-fold), PmrB (2.9-fold), and PmrC (5.5-fold) were highly expressed in the XDR strain, a finding consistent with an established mechanism of colistin resistance, while the lipid A biosynthesis enzymes LpxA, LpxC, and LpxD showed no significant difference between the XDR and MDR strains (Figure 3C).

Metabolic Changes Among the MDR, XDR, and DS Strains

Untargeted metabolomics via UHPLC-MS/MS identified 747 putatively annotated metabolites from the MDR, XDR, and DS strains: 454 in positive mode and 293 in negative mode. PCA showed clear separation among the three groups in both modes (Figure S2). DEMs were identified using VIP > 1, FC > 2 or < 0.5, and $p < 0.05$. Compared to the DS strain, the MDR strain had 98 up-regulated and 88 down-regulated metabolites (Figure 4A), while the XDR strain had 113 up-

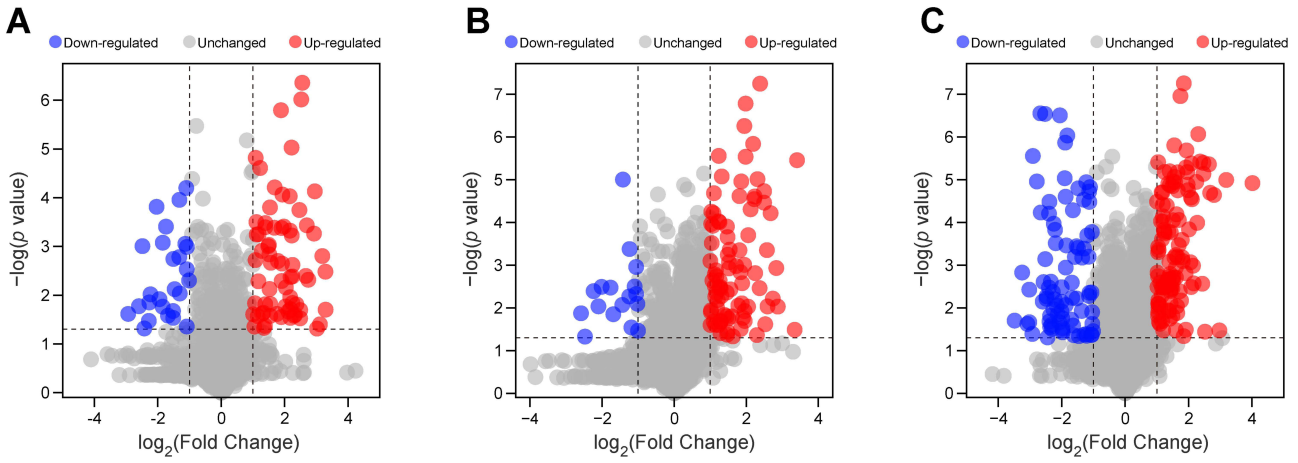

Figure 1 Volcano plots of the DEPs among the MDR, XDR, and DS strains. (**A**–**C**) Volcano plots comparing protein expression in MDR vs DS (**A**), XDR vs DS (**B**), and XDR vs MDR (**C**) strains. Red dots indicated significantly up-regulated proteins (FC > 2, $p < 0.05$), and blue dots indicated significantly down-regulated proteins (FC < 0.5, $p < 0.05$).

https://doi.org/10.2147/IDR.S573066

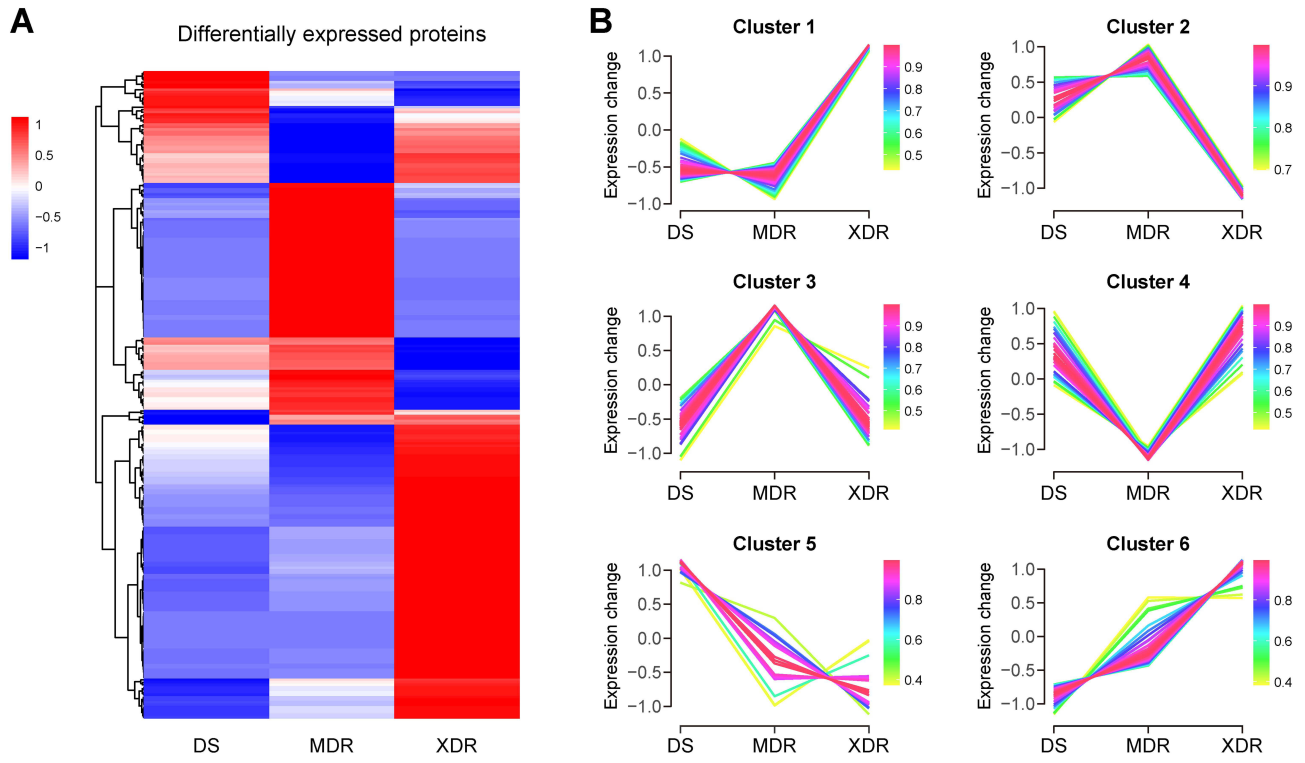

Figure 2 Clustering analysis of the DEPs across *A. baumannii* resistance phenotypes. (**A**) Hierarchical clustering heatmap displaying Z-score-normalized relative intensities of 260 DEPs in the DS, MDR, and XDR strains. Color scale: red = upregulated, blue = downregulated. (**B**) Fuzzy c-means clustering of DEP expression patterns. Colors indicate cluster membership values.

regulated and 99 down-regulated metabolites (Figure 4B). Compared to the MDR strain, the XDR strain had 78 elevated and 116 lower metabolites (Figure 4C). DEMs for each comparison were detailed in Tables S6–S8.

ClassyFire categorized the DEMs into 10 categories, with lipids and lipid-like molecules, nucleosides/nucleotides/analogues, organic acids/derivatives, and organoheterocyclic compounds being the most prevalent (Figure 4D). Pathway enrichment analysis indicated involvement in purine metabolism for all three comparisons (Figure 5A–C). Importantly, DEMs associated with colistin resistance were involved in glycerophospholipid metabolism, starch/sucrose metabolism, and glutathione metabolism (Figure 5C).

Analysis of Significant Metabolic Perturbations Associated with Colistin Resistance

Lipids and lipid-like molecules were significantly perturbed in this colistin-resistant *A. baumannii* strain, as illustrated in Figure 4D. Specifically, the XDR strain showed significantly lower relative abundance of several lysophosphatidylcholine (lysoPE), lysophosphatidylethanolamine (LPE), phosphatidylethanolamine (PE), phosphatidylcholine (PC), and lysophosphatidylcholine (LPC) compared to the MDR strain (Figure 6). Conversely, 3 species of LPE and lysophosphatidic acid (LPA) were up-regulated in the XDR strain. Additionally, the relative abundance levels of fatty acids/conjugates were substantially decreased in the XDR strain.

Discussion

The escalating prevalence of colistin-resistant *A. baumannii*, particularly XDR-CRAB strains, underscores the urgent need to unravel the molecular adaptations driving resistance in clinically relevant settings. This initial, high-resolution study employed integrated TMT-proteomics and untargeted metabolomics comparing three representative isolates (DS, MDR-CRAB, and XDR-CRAB) to establish a hypothesis-generating blueprint of the molecular differences associated with high-level colistin resistance. Our analysis revealed a complex interplay of proteomic and metabolomic changes in

https://doi.org/10.2147/IDR.S573066

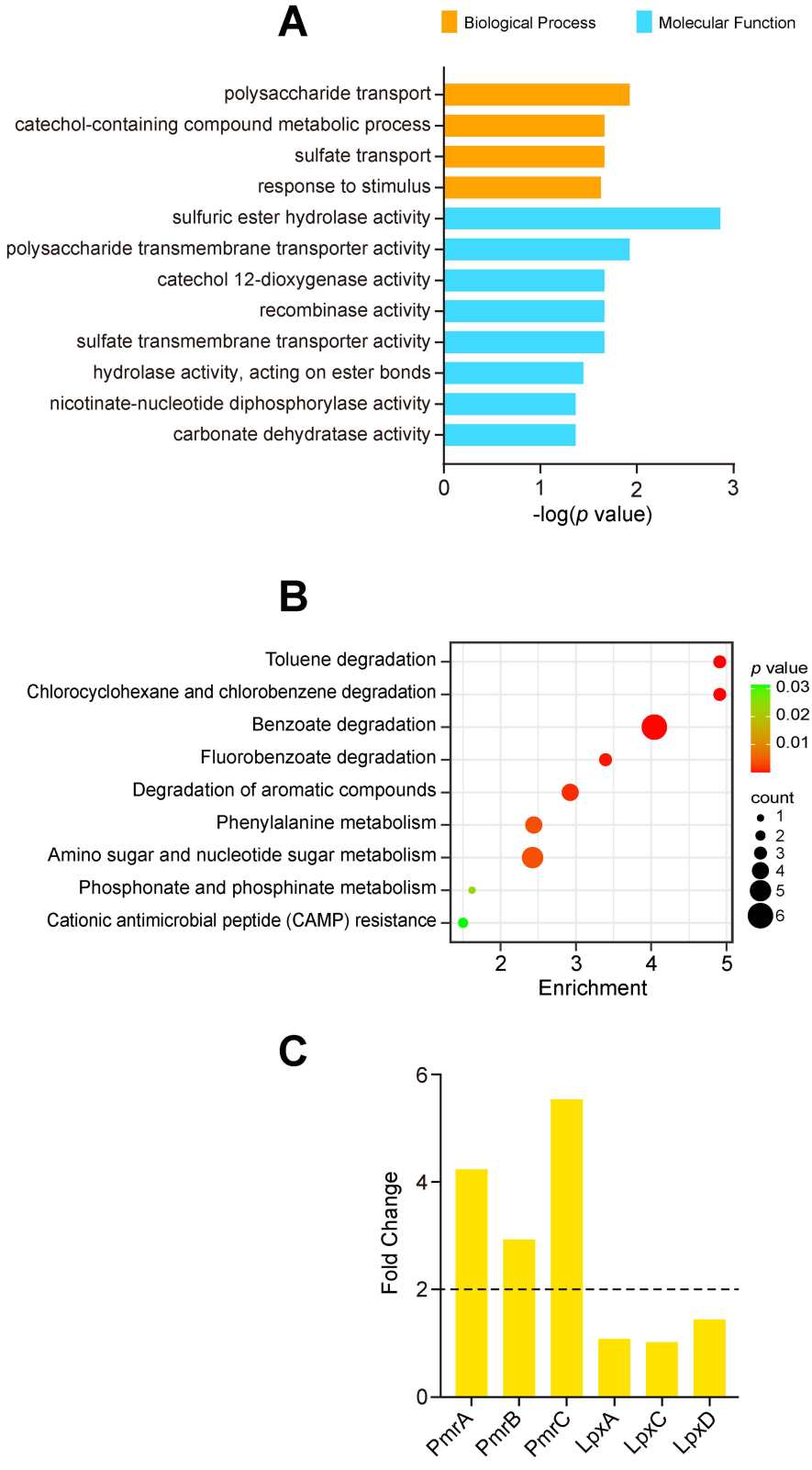

Figure 3 Functional Analysis of Colistin-Resistance-Associated DEPs. (**A**) GO enrichment of biological processes and molecular functions in Clusters 1 and 2. (**B**) KEGG pathway enrichment analysis. (**C**) Fold-change in lipid A modification and biosynthesis proteins (XDR vs MDR). Dashed line at FC = 2.

https://doi.org/10.2147/IDR.S573066

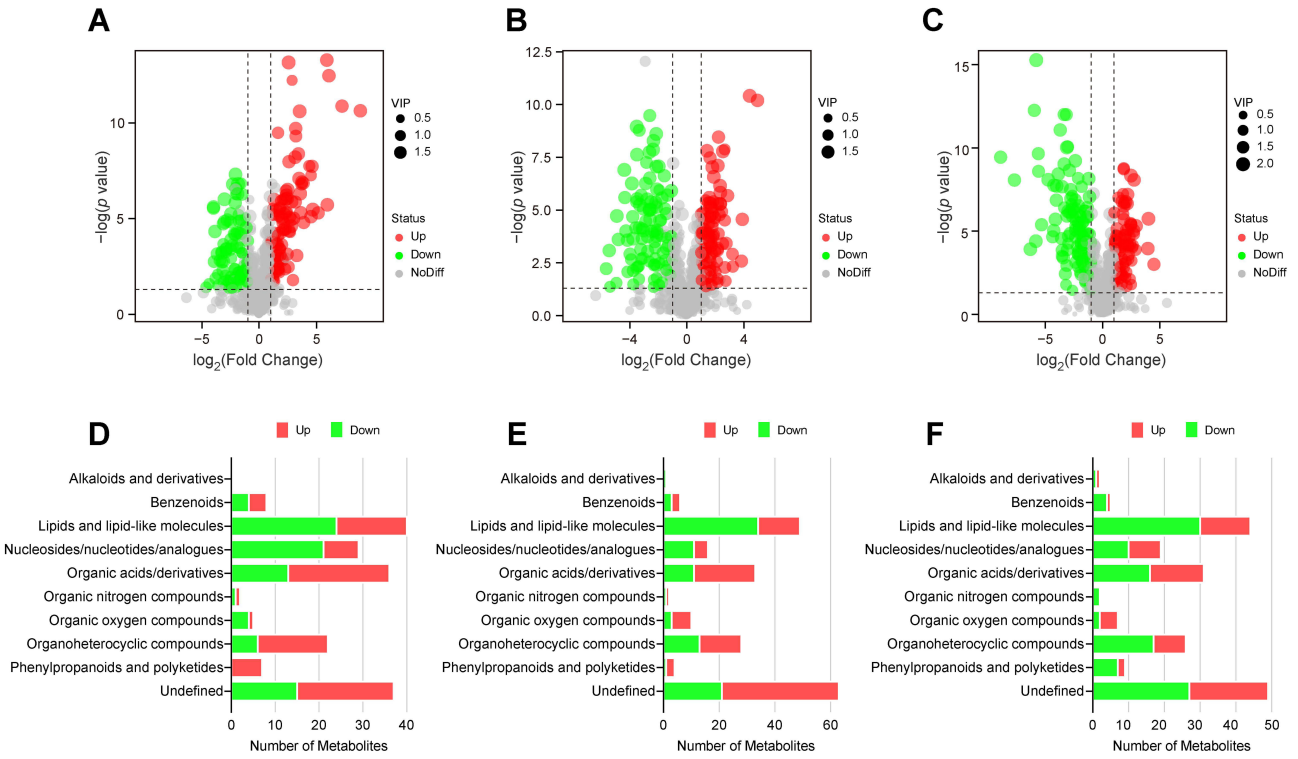

Figure 4 Metabolic changes in the MDR, XDR, and DS strains. (**A**–**C**) Volcano plots showing DEMs in MDR vs DS (**A**), XDR vs DS (**B**), and XDR vs MDR (**C**) strains. Red dots indicated up-regulated DEMs (VIP > 1, FC > 2, $p < 0.05$); green dots indicated down-regulated DEMs (VIP > 1, FC < 0.5, $p < 0.05$); gray dots indicated metabolites not significantly regulated. (**D**–**F**) ClassyFire functional classification of DEMs in MDR vs DS (**D**), XDR vs DS (**E**), and XDR vs MDR (**F**) strains. Red bars indicated number of up-regulated DEMs; green bars indicated down-regulated DEMs.

the XDR strain. Proteomic analysis identified 260 DEPs across these strains, with 98 DEPs showing strong association with the colistin-resistant phenotype. Functional enrichment analyses, including GO and KEGG, revealed the involvement of these key DEPs in diverse metabolic and transport processes, such as polysaccharide and sulfate transport, aromatic compound degradation, and crucially, CAMP resistance, which was largely consistent with the significantly upregulated lipid A modification system in the XDR strain. Metabolomic analysis further identified 747 metabolites, revealing substantial metabolic distinctions among the strains. Lipids and lipid-like molecules represented the most significantly altered metabolite class, and the XDR strain displayed notably reduced relative abundance of several glycerophospholipids, as well as fatty acids and conjugates, when compared to the MDR strain, which strongly suggests cell membrane remodeling. Pathway enrichment analysis implicated several key metabolic routes, including purine, glycerophospholipid, starch/sucrose, and glutathione metabolism in colistin resistance. Collectively, these correlative findings suggest toward a multifaceted colistin resistance strategy involving *PmrCAB*-mediated lipid A modification, cell membrane remodeling, and metabolic alterations. The identified DEPs and DEMs represent promising candidate targets for subsequent targeted validation studies necessary to confirm their causal role in colistin survival.

The striking upregulation of the *pmrCAB*-encoded lipid A modification system (PmrA, 4.2-fold; PmrB, 2.9-fold; PmrC, 5.5-fold) in the XDR strain compared to MDR is consistent with the known mechanism conferring CAMP resistance.[9,10] PmrA and PmrB constitute a two-component regulatory system that allows bacteria to detect and react to environmental signals, while PmrC is a transferase that adds PEtN to lipid A.[9,10] This modification reduces the net negative charge of lipid A, thereby decreasing its affinity for the cationic peptide colistin, a process regulated by the PmrA/PmrB system.[9,10] However, while the Pmr proteins were highly upregulated, the specific genetic mechanism driving this expression (eg, a mutation in *pmrB* or its upstream regulators) remains unverified in the absence of whole-genome sequencing (WGS) data for this clinical isolate. Future WGS of this strain is warranted to fully contextualize these proteomic shifts. Beyond this well-established modification system, our proteomics identified essential DEPs coordinating a multifaceted resistance strategy. Fuzzy c-means clustering identified two key DEP clusters: Cluster 1

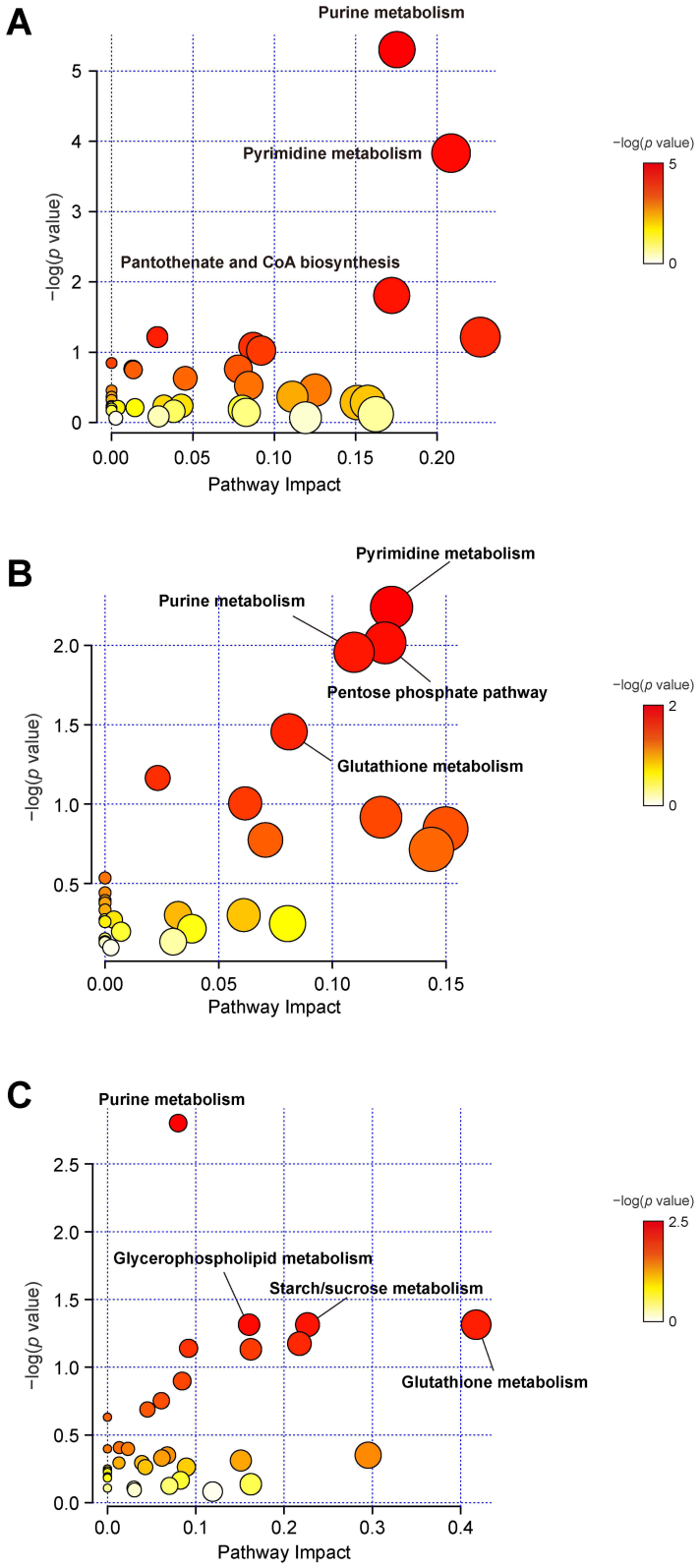

Figure 5 Pathway enrichment analysis of the DEMs. (**A**–**C**) Pathway enrichment for DEMs in MDR vs DS (**A**), XDR vs DS (**B**), and XDR vs MDR (**C**) strains. Dot size and color indicated the number and enrichment level of the DEMs in each pathway.

https://doi.org/10.2147/IDR.S573066

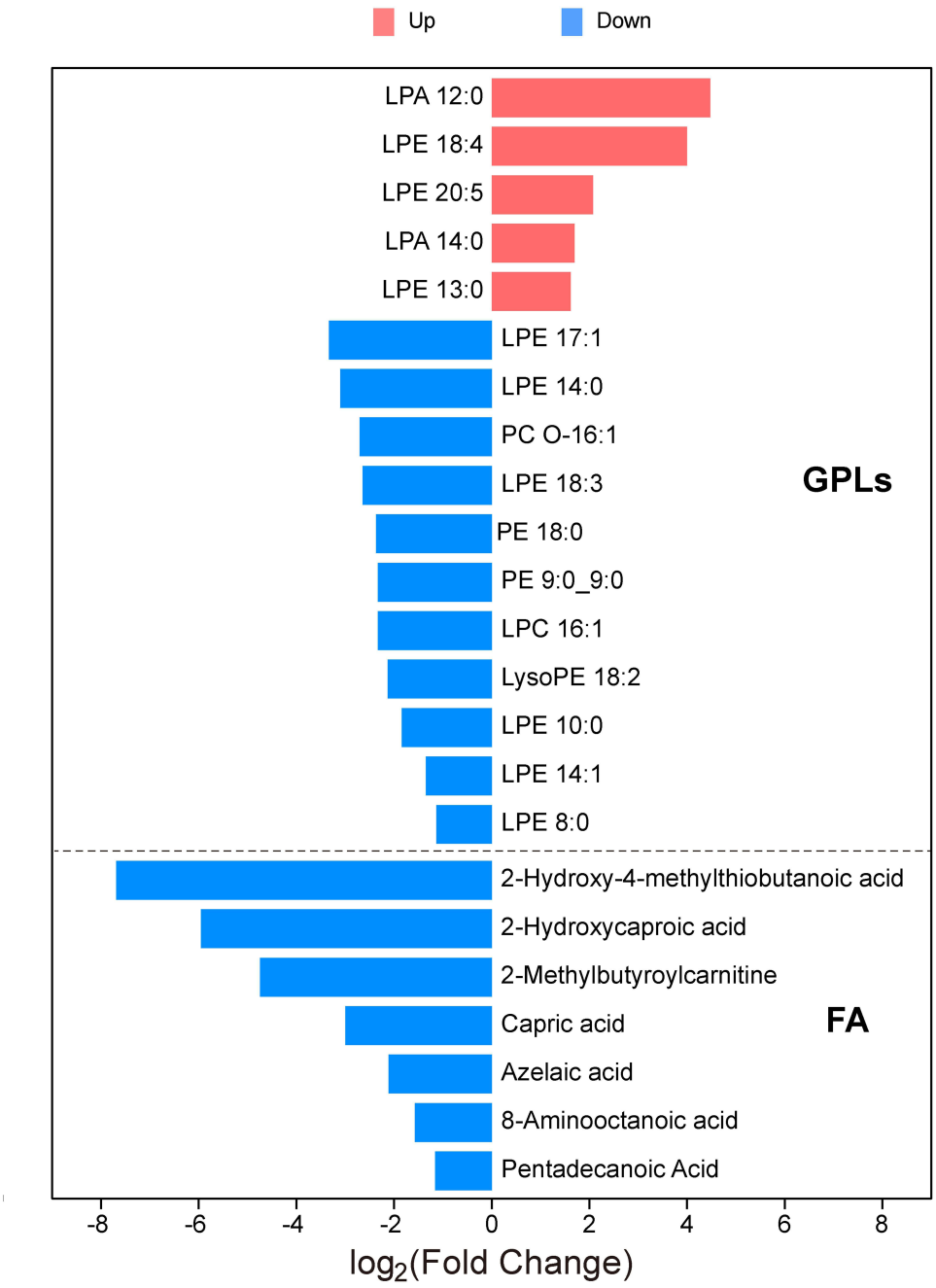

Figure 6 Significantly changed lipids in the colistin-resistant XDR strain. Log2 fold changes (XDR vs MDR) of significantly altered lipids. Red bars indicated increased abundance in the XDR strain; blue bars indicated decreased abundance.

Abbreviations: LysoPE, lysophosphatidylcholine; PE, phosphatidylethanolamine; LPE, lysophosphatidylethanolamine; PC, phosphatidylcholine; LPC, lysophosphatidylcholine; LPA, lysophosphatidic acid; GPLs, glycerophospholipids; FA, fatty acids/conjugates.

(73 upregulated proteins in the XDR strain) and Cluster 2 (25 downregulated proteins). Functional enrichment analyses revealed a coordinated adaptation network involving interconnected transport, metabolic, and stimulus response pathways. This was particularly evident in the significant enrichment of pathways associated with polysaccharide transport, suggesting modifications of the cell envelope, potentially contributing to the robust biofilm formation often observed in resistant strains.[17] Simultaneously, catechol-containing compound metabolic process was also significantly enriched. Given that catechol derivatives are known to function as siderophores to facilitate iron acquisition under stress conditions,[18] this enrichment suggested an active mobilization of iron-scavenging mechanisms. It is widely recognized

that antibiotic resistance mutations frequently incur a fitness cost, manifesting as reduced growth or competitiveness, which can stem from the metabolic burden of maintaining resistance mechanisms.[19] Specifically for colistin resistance, studies have demonstrated that the acquisition of resistance determinants, such as the *mcr-1* gene or mutations in the *pmrCAB* system, can impose significant physiological constraints.[20,21] Our proteomic observation of concurrent upregulation in both the *pmrCAB* system and iron acquisition related pathways suggested a complex and potentially costly physiological adaptation. Since colistin-resistant *A. baumannii* has been reported to show impaired growth under iron-limiting conditions,[21] our proteomic data suggested a simultaneous investment in colistin defense and iron scavenging, which indicated an active compensatory effort by the XDR strain to mitigate this known fitness cost. The potential trade-off between colistin resistance and iron acquisition efficiency warrants dedicated experimental confirmation. Furthermore, sulfate transport and aromatic compound degradation pathways were activated, potentially aiding in detoxifying colistin-induced oxidative byproducts or maintaining energy homeostasis under antibiotic stress.[22] The concurrent enrichment of pathways related to phosphonate/phosphinate, phenylalanine, and amino sugar and nucleotide sugar metabolism, further underscored the observed metabolic plasticity utilized by the XDR strain to maintain cell wall integrity and biofilm dynamics.[23–26] Finally, transmembrane transporter and enzyme enrichment underscored their indispensable role in colistin resistance, collectively illustrating *A. baumannii*'s remarkable adaptability through integrated structural and metabolic plasticity.

The metabolomic profiling of *A. baumannii* strains with varying colistin resistance levels (DS, MDR, XDR) revealed profound metabolic reprogramming. In line with previous studies,[27–31] we found constituted the most abundant class of altered metabolites across all comparisons of DS and drug-resistant *A. baumannii* strains, indicating that perturbations in lipid metabolism might play a crucial role in the antibiotic resistance phenotype. Notably, the XDR strain exhibited significant perturbations in glycerophospholipid metabolism, with lower relative levels of several glycerophospholipid species (PE, PC, LPC, LPE, lysoPE) and various fatty acids/conjugates compared to the MDR strain. Glycerophospholipids and fatty acids are important components of cell membrane and essential for outer membrane integrity and bacterial survival.[32] However, our observation of specific reduced lipid levels contrasted with reports of lipid accumulation in resistant strains.[27–31] One possible explanation for the observed reduction in specific glycerophospholipids and fatty acids is an active remodeling of membrane composition aimed at altering its biophysical properties. It is well established that membrane lipid composition is intricately linked to its fluidity and permeability, and organisms can precisely tune these properties through lipidomic adaptations.[32] Notably, lipidome remodeling in response to stress has been directly observed in *A. baumannii*. For instance, studies have shown that *A. baumannii* persister cells alter their lipid profiles to increase membrane rigidity, likely to reduce permeability and enhance survival under antibiotic pressure.[33] Similarly, clinical strains of *A. baumannii* modulate glycerophospholipid composition to maintain membrane fluidity across different temperatures.[34] Therefore, we hypothesize that the distinct lipid profile of our colistin-resistant XDR strain may represent a similar adaptive strategy. The reduction in certain membrane lipids could be a targeted effort to decrease membrane fluidity (increase rigidity), thereby directly impeding the insertion and disruptive action of colistin into the lipid bilayer. Confirmation of this specific hypothesis, however, requires direct experimental measurement of membrane fluidity and permeability in future studies. In addition to the major lipid classes, we observed differential expression in specific LPE and LPA species. While these molecules are well-established mediators of inflammatory regulation in eukaryotic system,[35] their precise role in bacterial stress responses remains speculative, warranting focused investigation in future studies. Pathway analysis confirmed the consistent involvement of purine metabolism across all three groups, suggesting a generalized adaptive response to cellular stress. The increased demand for purines may correlate with an increased need to maintain nucleotide pools for DNA repair and replication, potentially mitigating damage induced by colistin or other cellular stressors.[36] In addition, the perturbation of starch/sucrose metabolism in the XDR strain suggested a potential link between carbohydrate utilization and biofilm formation, a hypothesis partially supported by epidemiological studies on *A. baumannii* persistence in hospital environments.[14,37] Finally, we observed a significant enrichment of DEMs involved in glutathione metabolism, suggesting that alterations in oxidative stress responses might also contribute to the colistin resistance phenotype. Colistin is known to induce the accumulation of reactive oxygen species (ROS), leading to rapid bacterial cell death.[38,39] Glutathione is a major antioxidant and plays a critical role in protecting cells from oxidative

stress.[40,41] The observed upregulation of glutathione metabolism in the XDR strain might represent a compensatory response to oxidative stress induced by colistin exposure, enabling the cell to neutralize ROS and mitigate the cytotoxic effects of the antibiotic.[42,43] It is important to note that our metabolomic findings were derived from untargeted metabolomics, an exploratory approach suited for hypothesis generation. Consequently, the specific lipid changes reported here should be regarded as candidate signatures and testable hypotheses. Their precise quantification, confident annotation (particularly for lipid isomers), and functional roles require definitive validation through targeted lipidomics and subsequent mechanistic studies.

Our study had certain limitations. Firstly, the in-depth analysis of a single representative XDR isolate, while valuable for generating focused hypotheses, inherently limits the generalizability of the proposed resistance mechanisms. The findings require validation across a larger, genetically diverse panel of clinical *A. baumannii* isolates to assess their prevalence and universality. Secondly, the correlative nature of our multi-omics data, without accompanying genetic manipulations (eg, gene knockout, complementation or overexpression), precludes the establishment of direct causality. Future studies integrating functional genomics are essential to confirm the mechanistic roles of the identified DEPs and metabolic pathways. Thirdly, the experimental conditions (nutrient-rich LB medium) represent a substantial simplification compared to the complex host environment during infection. It remains to be determined whether the observed metabolic reprogramming and membrane remodeling occur similarly under host-relevant stresses such as nutrient limitation, immune pressure, or within biofilms. Fourthly, as acknowledged in the metabolomics discussion, the untargeted approach used here is superb for discovery but has limitations in precise quantification and isomer discrimination. The specific lipid changes reported are therefore considered strong candidate signatures that must be confirmed and absolutely quantified via targeted lipidomics. Finally, the lack of temporal data provides only a static snapshot. Longitudinal multi-omics analyses tracking adaptation under sub-inhibitory colistin pressure would be invaluable for elucidating the dynamic evolutionary trajectory of resistance acquisition.

Despite its limitations, this study offers significant value by generating a high-resolution molecular blueprint of colistin-resistant *A. baumannii* using integrated proteomics and metabolomics on a highly resistant clinical isolate. We propose a multifaceted resistance model that moves beyond single determinants to encompass lipid A modification, membrane remodeling, and metabolic adaptation. Given the rapid evolution of XDR-CRAB, these focused hypotheses are essential to guide efficient functional studies. Thus, our study serves as a foundational resource, delineating clear experimental paths to establish causal mechanisms and explore novel therapeutic targets.

In conclusion, our integrated proteomic and metabolomic analysis of a single clinical XDR-CRAB strain provides a high-resolution molecular portrait and a wealth of testable hypotheses regarding colistin resistance. The candidate mechanisms proposed here, including PmrCAB-mediated lipid A modification, cell membrane remodeling, and metabolic reprogramming, require further validation through genetic experiments and across a panel of independent clinical isolates to establish their universality. This study serves as a foundational resource; if validated, these findings could offer potential targets for novel therapeutic strategies.

Abbreviations

A. Baumannii, Acinetobacter baumannii; CAMP, cationic antimicrobial peptide; CLSI, Clinical and Laboratory Standards Institute; CRAB, carbapenem-resistant *A. baumannii*; CV, coefficient of variation; DEMs, differentially expressed metabolites; DEPs, differentially expressed proteins; DS, drug-sensitive; FC, fold change; FDR, false discovery rate; GO, Gene Ontology; KEGG, Kyoto Encyclopedia of Genes and Genomes; LPA, lysophosphatidic acid; LPC, lysophosphatidylcholine; LPE, lysophosphatidylethanolamine; LPS, lipopolysaccharides; lysoPE, lysophosphatidylcholine; MDR, multidrug-resistant; PC, phosphatidylcholine; PCA, principal component analysis; PDR, pan-drug-resistant; PE, phosphatidylethanolamine; PEtN, phosphoethanolamine; ROS, reactive oxygen species; TMT, tandem mass tag; VIP, variable importance in the projection; XDR, extensively drug-resistant.

Data Sharing Statement

The data used to support the findings of this study are available from the corresponding author upon request.

Ethics Statement

Not applicable. This work involved only bacterial strains and did not involve human subjects or animals.

Funding

This work was financially supported by grants from the National Natural Science Foundation of China (Grant Number 82302529), the Guangdong Basic and Applied Basic Research Foundation (Grant Number 2023A1515012421), the Guangzhou Science and Technology Plan Project (Grant Number 2025A04J5237 and 202201010177), and the Doctoral Voyage Project of Guangzhou Science and Technology Bureau (Grant Number SL2023A04J00962).

Disclosure

The authors declare that the research was conducted in the absence of any commercial or financial relationships that could be construed as a potential conflict of interest.

References

1. Miller WR, Arias CA. ESKAPE pathogens: antimicrobial resistance, epidemiology, clinical impact and therapeutics. *Nat Rev Microbiol*. 2024;22(10):598–616. doi:10.1038/s41579-024-01054-w
2. García-Garmendia JL, Ortiz-Leyba C, Garnacho-Montero J, et al. Risk factors for Acinetobacter baumannii nosocomial bacteremia in critically ill patients: a cohort study. *Clin Infect Dis*. 2001;33(7):939–946. doi:10.1086/322584
3. Spellberg B, Rex JH. The value of single-pathogen antibacterial agents. *Nat Rev Drug Discov*. 2013;12(12):963. doi:10.1038/nrd3957-c1
4. China Antimicrobial Surveillance Network. CHINET. Available from: www.chinets.com. Accessed September 3, 2025.
5. Li J, Nation RL, Turnidge JD, et al. Colistin: the re-emerging antibiotic for multidrug-resistant gram-negative bacterial infections. *Lancet Infect Dis*. 2006;6(9):589–601.
6. Cai Y, Chai D, Wang R, et al. Colistin resistance of Acinetobacter baumannii: clinical reports, mechanisms and antimicrobial strategies. *J Antimicrob Chemother*. 2012;67(7):1607–1615. doi:10.1093/jac/dks084
7. Cain AK, Hamidian M. Portrait of a killer: uncovering resistance mechanisms and global spread of Acinetobacter baumannii. *PLoS Pathog*. 2023;19(8):e1011520. doi:10.1371/journal.ppat.1011520
8. Moffatt JH, Harper M, Harrison P, et al. Colistin resistance in Acinetobacter baumannii is mediated by complete loss of lipopolysaccharide production. *Antimicrob Agents Chemother*. 2010;54(12):4971–4977. doi:10.1128/AAC.00834-10
9. Park YK, Choi JY, Shin D, et al. Correlation between overexpression and amino acid substitution of the PmrAB locus and colistin resistance in Acinetobacter baumannii. *Int J Antimicrob Agents*. 2011;37(6):525–530. doi:10.1016/j.ijantimicag.2011.02.008
10. Charretier Y, Diene SM, Baud D, et al. Colistin heteroresistance and involvement of the PmrAB regulatory system in Acinetobacter baumannii. *Antimicrob Agents Chemother*. 2018;62(9):e00788–18. doi:10.1128/AAC.00788-18
11. Deris ZZ, Akter J, Sivanesan S, et al. A secondary mode of action of polymyxins against Gram-negative bacteria involves the inhibition of NADH-quinone oxidoreductase activity. *J Antibiot*. 2014;67(2):147–151. doi:10.1038/ja.2013.111
12. Khuntayaporn P, Thirapanmethee K, Chomnawang MT. An update of mobile colistin resistance in non-fermentative gram-negative Bacilli. *Front Cell Infect Microbiol*. 2022;12:882236. doi:10.3389/fcimb.2022.882236
13. Wang X, Zhang L, Chen H, et al. Rational proteomic analysis of a new domesticated Klebsiella pneumoniae x546 producing 1,3-Propanediol. *Front Microbiol*. 2021;12:770109. doi:10.3389/fmicb.2021.770109
14. Guo R, Luo X, Liu J, et al. Mass spectrometry based targeted metabolomics precisely characterized new functional metabolites that regulate biofilm formation in Escherichia coli. *Anal Chim Acta*. 2021;1145:26–36. doi:10.1016/j.aca.2020.12.021
15. Hao L, Yang X, Chen H, et al. Distribution and drug resistance of bacterial infection in hospitalized patients at the respiratory department before and after the COVID-19 pandemic in Guangzhou, China. *Microorganisms*. 2023;11(10):2542. doi:10.3390/microorganisms11102542
16. Clinical and Laboratory Standards Institute. *Performance Standards for Antimicrobial Susceptibility Testing M100-Ed33*. Wayne, PA, USA: CLSI; 2023.
17. Tiwari M, Panwar S, Kothidar A, et al. Rational targeting of Wzb phosphatase and Wzc kinase interaction inhibits extracellular polysaccharides synthesis and biofilm formation in Acinetobacter baumannii. *Carbohydr Res*. 2020;492:108025. doi:10.1016/j.carres.2020.108025
18. Miethke M, Marahiel MA. Siderophore-based iron acquisition and pathogen control. *Microbiol Mol Biol Rev*. 2007;71(3):413–451. doi:10.1128/MMBR.00012-07
19. Andersson DI. The biological cost of mutational antibiotic resistance: any practical conclusions? *Curr Opin Microbiol*. 2006;9(5):461–465. doi:10.1016/j.mib.2006.07.002
20. Guo Z, Feng S, Liang L, et al. Assessment of the reversibility of resistance in the absence of antibiotics and its relationship with the resistance gene's fitness cost: a genetic study with mcr-1. *Lancet Microbe*. 2024;5(8):100846. doi:10.1016/S2666-5247(24)00052-1
21. López-Rojas R, García-Quintanilla M, Labrador-Herrera G, et al. Impaired growth under iron-limiting conditions associated with the acquisition of colistin resistance in Acinetobacter baumannii. *Int J Antimicrob Agents*. 2016;47(6):473–477. doi:10.1016/j.ijantimicag.2016.03.010
22. Alkasir R, Ma Y, Liu F, et al. Characterization and transcriptome analysis of Acinetobacter baumannii persister cells. *Microb Drug Resist*. 2018;24(10):1466–1474. doi:10.1089/mdr.2017.0341
23. Silkenath B, Kläge D, Altwein H, et al. Phosphonate and Thiasugar Analogues of Glucosamine-6-phosphate: activation of the glmS Riboswitch and Antibiotic Activity. *ACS Chem Biol*. 2023;18(10):2324–2334. doi:10.1021/acschembio.3c00452
24. Sheppard DC, Howell PL. Biofilm exopolysaccharides of pathogenic fungi: lessons from bacteria. *J Biol Chem*. 2016;291(24):12529–12537. doi:10.1074/jbc.R116.720995

25. Mitchell KF, Zarnowski R, Sanchez H, et al. Community participation in biofilm matrix assembly and function. *Proc Natl Acad Sci U S A*. 2015;112(13):4092–4097. doi:10.1073/pnas.1421437112
26. Shen F, Ge C, Yuan P. Metabolomics study reveals inhibition and metabolic dysregulation in Staphylococcus aureus Planktonic cells and biofilms induced by Carnosol. *Front Microbiol*. 2020;11:538572. doi:10.3389/fmicb.2020.538572
27. Han ML, Liu X, Velkov T, et al. Comparative metabolomics reveals key pathways associated with the synergistic killing of colistin and sulbactam combination against multidrug-resistant Acinetobacter baumannii. *Front Pharmacol*. 2019;10:754. doi:10.3389/fphar.2019.00754
28. Chen X, Tian J, Luo C, et al. Cell membrane remodeling mediates Polymyxin B resistance in Klebsiella pneumoniae: an integrated proteomics and metabolomics study. *Front Microbiol*. 2022;13:810403. doi:10.3389/fmicb.2022.810403
29. Jasim R, Han ML, Zhu Y, et al. Lipidomic analysis of the outer membrane vesicles from paired polymyxin-susceptible and -resistant Klebsiella pneumoniae clinical isolates. *Int J Mol Sci*. 2018;19(8):2356. doi:10.3390/ijms19082356
30. Li H, Wang Y, Meng Q, et al. Comprehensive proteomic and metabolomic profiling of mcr-1-mediated colistin resistance in Escherichia coli. *Int J Antimicrob Agents*. 2019;53(6):795–804. doi:10.1016/j.ijantimicag.2019.02.014
31. Aye SM, Galani I, Han ML, et al. Lipid A profiling and metabolomics analysis of paired polymyxin-susceptible and -resistant MDR Klebsiella pneumoniae clinical isolates from the same patients before and after colistin treatment. *J Antimicrob Chemother*. 2020;75(10):2852–2863. doi:10.1093/jac/dkaa245
32. Sohlenkamp C, Geiger O. Bacterial membrane lipids: diversity in structures and pathways. *FEMS Microbiol Rev*. 2016;40(1):133–159. doi:10.1093/femsre/fuv008
33. Vergoz D, Schaumann A, Schmitz I, et al. Lipidome of Acinetobacter baumannii antibiotic persister cells. *Biochim Biophys Acta Mol Cell Biol Lipids*. 2024;1869(7):159539. doi:10.1016/j.bbalip.2024.159539
34. Dessenne C, Ménart B, Acket S, et al. Lipidomic analyses reveal distinctive variations in homeoviscous adaptation among clinical strains of Acinetobacter baumannii, providing insights from an environmental adaptation perspective. *Microbiol Spectr*. 2024;12(10):e0075724. doi:10.1128/spectrum.00757-24
35. Jiang S, Yang H, Li M. Emerging roles of lysophosphatidic acid in macrophages and inflammatory diseases. *Int J Mol Sci*. 2023;24(15):12524. doi:10.3390/ijms241512524
36. Kohanski MA, Dwyer DJ, Hayete B, et al. A common mechanism of cellular death induced by bactericidal antibiotics. *Cell*. 2007;130(5):797–810. doi:10.1016/j.cell.2007.06.049
37. Doughty EL, Liu H, Moran RA, et al. Endemicity and diversification of carbapenem-resistant Acinetobacter baumannii in an intensive care unit. *Lancet Reg Health West Pac*. 2023;37:100780. doi:10.1016/j.lanwpc.2023.100780
38. Yu Z, Zhu Y, Qin W, et al. Oxidative stress induced by Polymyxin E is involved in rapid killing of Paenibacillus polymyxa. *Biomed Res Int*. 2017;2017:5437139. doi:10.1155/2017/5437139
39. Ajiboye TO, Skiebe E, Wilharm G. Phenolic acids potentiate colistin-mediated killing of Acinetobacter baumannii by inducing redox imbalance. *Biomed Pharmacother*. 2018;101:737–744. doi:10.1016/j.biopha.2018.02.051
40. Forman HJ, Zhang H, Rinna A. Glutathione: overview of its protective roles, measurement, and biosynthesis. *Mol Aspects Med*. 2009;30(1–2):1–12. doi:10.1016/j.mam.2008.08.006
41. Wu G, Fang YZ, Yang S, et al. Glutathione metabolism and its implications for health. *J Nutr*. 2004;134(3):489–492. doi:10.1093/jn/134.3.489
42. Rodgers D, Le C, Pimentel C, et al. Histone-like nucleoid-structuring protein (H-NS) regulatory role in antibiotic resistance in Acinetobacter baumannii. *Sci Rep*. 2021;11(1):18414. doi:10.1038/s41598-021-98101-w
43. Rath S, Das S. Oxidative stress-induced DNA damage and DNA repair mechanisms in mangrove bacteria exposed to climatic and heavy metal stressors. *Environ Pollut*. 2023;339:122722. doi:10.1016/j.envpol.2023.122722